Research article

Jin Xiang, Yi Xu*, Jing-Dong Chen and Sheng Lan*

Tailoring the spatial localization of bound state in the continuum in plasmonic-dielectric hybrid system

https://doi.org/10.1515/nanoph-2019-0341
Received September 2, 2019; revised October 25, 2019; accepted October 26, 2019

Abstract: Bound states in the continuum (BIC) are considered as an effective means to dramatically elongate the trapping time of light. However, light-matter interaction depends not only on the life-time of an optical mode, but also on its mode volume. Therefore, increasing the life-time of an optical mode and minimizing the mode volume simultaneously, utilizing the BIC resembles a promising way for enhancing light-matter interaction. Herein, we have proposed a novel hybrid plasmonic-dielectric structure to manipulate the mode volume of BIC. For the Friedrich-Wintgen BIC, the electric field is strongly confined in the dielectric nanoparticle, leading to the considerable field enhancement compared with the single dielectric nanoparticle case. In contrast, strong localization of electric field can be achieved along the surface normal direction for the symmetry-protected BIC, leading to one order of magnitude reduction of mode volume in one unit cell compared with the conventional symmetry-protected BIC of all-dielectric structure. The proposed hybrid photonic system could provide an ideal flat platform for advanced manipulation of light-matter interaction.

***Corresponding authors: Yi Xu,** Department of Electronic Engineering, College of Information Science and Technology, Jinan University, 510632 Guangzhou, China, e-mail: yi.xu@osamember.org; and **Sheng Lan,** Guangdong Provincial Key Laboratory of Nanophotonic Functional Materials and Devices, School of Information and Optoelectronic Science and Engineering, South China Normal University, Guangzhou 510006, China, e-mail: slan@scnu.edu.cn
Jin Xiang: Guangdong Provincial Key Laboratory of Nanophotonic Functional Materials and Devices, School of Information and Optoelectronic Science and Engineering, South China Normal University, Guangzhou 510006, China.
https://orcid.org/0000-0003-0896-7526
Jing-Dong Chen: College of Physics and Information Engineering, Minnan Normal University, Zhangzhou, 363000, China

Keywords: bound state in the continuum; Mie resonance; nonlinear optical absorption; surface plasmon polaritons; dielectric-metal hybrid structure.

1 Introduction

Strongly localized electromagnetic field at the nanoscale is highly desirable for enhancing light-matter interaction [1–3]. As a result, surface plasmon polaritons (SPPs), which is accompanied by deep-subwavelength localization and dramatic enhancement of electric field at optical frequencies, have been widely employed to boost the strength of light-matter interaction [4]. Although plasmomic modes possess significant reduced mode volumes compared with photonic modes, their quality (Q) factors are usually quite low owing to the intrinsic absorption loss of metal, resembling a fundamental limit that endowed by the physics of plasmonics. Basically, the Q factors of plasmonic modes can be improved by using Wood's anomaly (WA) [5], where the improvement was achieved inevitably by scarificing the size of mode volume.

In principle, Mie resonances in dielectric nanoparticles with large refractive indices can be employed to release the Ohmic loss [6–9]. Although an improvement of Q factor can be achieved in such a wavelength scale nanoparticles, because of its dielectric nature, the realization of high Q factor resonance is still hindered by the radiation loss of corresponding electromagnetic multipole modes (i.e. scattering) of the high refractive index nanoparticle. Alternatively, the hybrid plasmonic-photonic system consisting of a semiconductor (CdSe) nanowire placed on a silver (Ag) film was demonstrated to be capable of neutralizing subwavelength localization and Ohmic loss simultaneously, resembling a versatile platform for engineering active light-matter interaction [10]. However, although such a two-dimensional subwavlength optical field confinement originated from the hybridization between photonic and plasmonic modes can be used to improve the Purcell factor of the hybrid system and eventually lead to

the lasing of the CdSe nanowire [11], the Q factor of the hybrid system is still limited. Similarly, the hybrid concept was used to boost the Purcell factor and generate efficient hot electron luminescence from a silicon (Si) nanowire coated with a thin Ag film [12]. Furthermore, such a strategy can be generalized to the three-dimensional case for realizing strong localization of optical field in particle-on-film systems where dielectric nanoparticles (such as Si nanospheres) supporting distinct Mie resonances were used [13, 14]. As an exemplary application, the significantly enhanced electric field mediated by the mirror-image-induced magnetic dipole mode was exploited to enhance Raman scattering and photoluminescence [15].

One of the efficient ways to boost the radiative Q factor can be relied on bound states in the continuum (BICs) that were firstly predicted in electronics by von Neumann and Wigner in 1929 [16]. It is not until 80 years later, the photonic analogue of BICs was proposed for the first time and now it became a vivid sub-research field in nanophotonics [17, 18]. For example, BICs of photonic crystal (PhC) slabs and metasurface structures provide flat photonic platforms for engineering BIC associated ultra-high-Q resonances [17–25], which enables the realization of various promising applications [6, 26, 27]. Basically, there are two interesting types of BICs observed in the PhC slabs, including symmetry-protected BIC (SP-BIC) [17, 18] and Friedrich-Wintgen BIC (FW-BIC) [28, 29] which was proposed in 2002 by Tikhodeev et al. The former type arises from the symmetry incompatibility between the localized mode and the incident wave of the continuum, while the latter type relies on the destructive interference between two scattering channels [30]. The SP-BIC can be accessed by either breaking the symmetry of the structure or the excitation [22]. For the FW-BIC, one can tune the Q factors of leaky resonance originated from such BIC by varying the structural parameters or excitation conditions [31, 32]. To date, for any structure that supports BICs, it should extend to an infinity in one spatial dimension at least. Therefore, the way to engineer electromagnetic field localization of BIC should be achieved in the orthogonal spatial dimensions. Very recently, a hybrid dielectric-metal structure composed of a dielectric waveguide and a metal grating, was proposed to realize BIC in a lossy system [33]. However, how different BIC modes can be used to shape the localization of electromagnetic near-field in the hybrid structure was yet to be addressed.

In this paper, we have proposed a novel dielectric-metal hybrid structure, which is formed by a periodic array of high-index dielectric nanoparticles sitting on a MgF_2/Ag/SiO_2 substrate, to manipulate the localization of electromagnetic field in one unit cell of the structure based on the SP-BIC and FW-BICs. It is found that the strong localization of electric field can be achieved either in the dielectric nanoparticles or in the nanoscale dielectric gap between the dielectric nanoparticle and the metal film. Giving the possibility to boost the Q factor and minimize the effective optical mode volume in one unit cell of the structure simultaneously, many fascinating nanophotonic applications can be anticipated based on such flat platforms, but not limited to lasing action at BIC [27], white light emission from indirect bandgap semiconductor [7] and light-matter interaction in low dimension system [3].

2 Results and discussion

The dielectric-metal hybrid structure proposed in this work is schematically shown in Figure 1A. In practice, there are many choices of dielectric (e.g. Si, Ge, GaAs etc.) and metallic (e.g. Au, Ag, Al etc.) materials for the hybrid structure. In this work, a hybrid structure is formed by a MgF_2 layer ($g = 25$ nm) sandwiched by a periodic array of Si nanopillars and a thin Ag film. As shown in Figure 1A, the Si nanopillars are arranged in a square lattice with a lattice constant l. The thickness of the nanoscale dielectric spacer layer (e.g. a MgF_2 layer with a refractive index $n = 1.38$) is $g = 25$ nm and the thickness for the Ag film is $t = 100$ nm. The hybrid structure sits on a glass substrate. Our results can be readily extended to other hybrid systems. As a first step, we have investigated the scattering of a single Si nanopillar with different substrates. We have neglected the optical loss of Si first (n = 3.4) and the dispersive and lossy case will be provided in the Supporting information. In Figure 1B, the extinction spectrum of a single Si nanopillar with a diameter $d = 200$ nm and a height $h = 190$ nm sitting on a silica (SiO_2) substrate ($n_{sub} = 1.45$) is presented, where the extinction is dominated by the contributions of MD and ED modes. When the thin Ag film and the nanoscale MgF_2 spacer layer are added to this system, the extinction spectrum of the Si nanopillar is modified dramatically, as shown in Figure 1C. In this case, the ED and MD induced in the Si nanopillar can also be evaluated [34, 35]. The existence of the Ag film will introduce the bianisotropic effect, which is corresponding to the excitation of a out-of-phase MD moment at the ED resonance near 720 nm in the Si nanopillar [35–37]. It is noticed that the MD moment contributes negatively to the total extinction in the presence of the Ag film, because of bianisotropic effect implying a destructive interference between the fields scattered by the ED and MD moments [36]. More importantly, such bianisotropic effect also results in

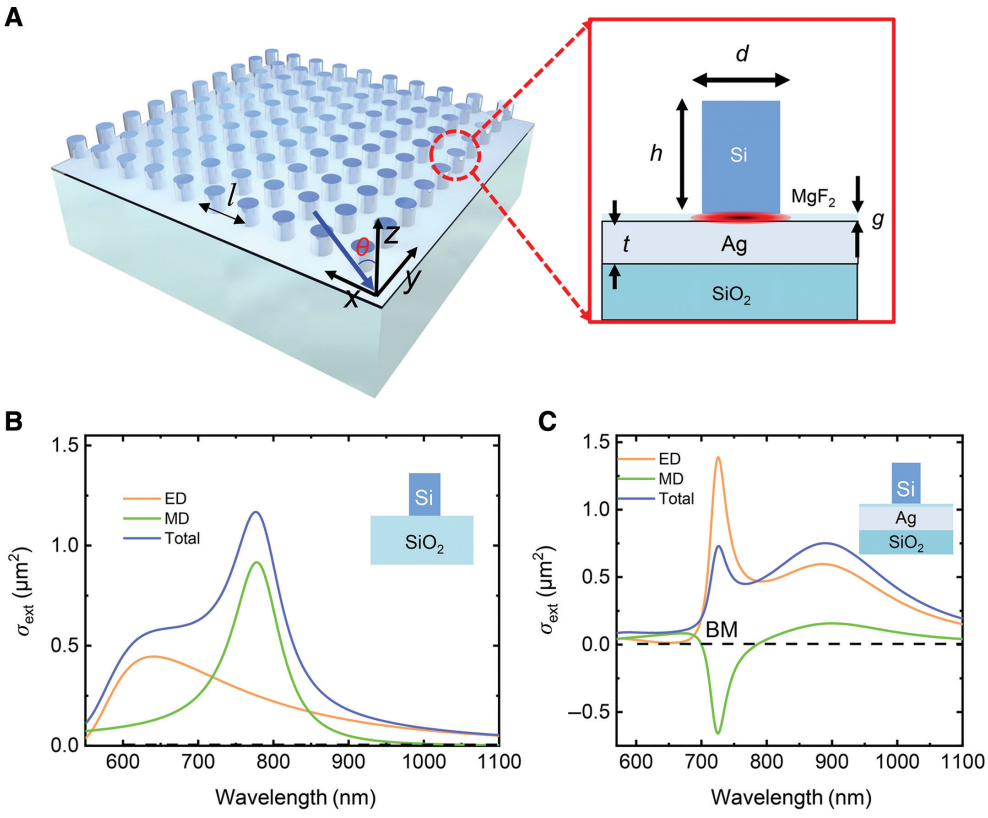

Figure 1: Optical response of a single Si nanoparticle on different substrates.
(A) Schematic of the hybrid plasmonic-photonic system investigated in this work. It is composed of a periodic array of Si nanopillars, a thin MgF_2 spacer layer, a thin Ag film and a SiO_2 substrate. l indicates the lattice constant. The detailed geometry parameters of the periodic structure are outlined in the inset. (B) and (C) Extinction spectra calculated for a single Si nanopillar with $d = 200$ nm and $h = 190$ nm placed on a SiO_2 and an $MgF_2/Ag/SiO_2$ substrate, respectively. In each case, the plane wave propagates along the -Z direction and the polarization is along the X-axis. The extinction spectrum has been decomposed into the contributions from the induced ED and MD moments.

the shrinkage of the ED resonance's line width [14], as clearly shown in Figure 1C.

The momentum-matching condition between the resonant modes excited in the hybrid structure and the incident light can be described by Bragg's coupling equation [38, 39]:

$$\mathbf{k}_0 \sin\theta \pm i\mathbf{G}_x \pm j\mathbf{G}_y = \mathbf{k}_{\text{mode}}, \tag{1}$$

where $\mathbf{k}_0$ is the wave vector of the incident light with an incident angle θ, $\mathbf{G}_x$ and $\mathbf{G}_y$ are the Bragg vectors associated with the two periodicities of the array, i and j are integers indicating the orders of the scattering event. The wave vectors of the SPP and WA modes ($\mathbf{k}_{\text{SPP}}$ and $\mathbf{k}_{\text{WA}}$) are given by $|\mathbf{k}_{\text{SPP}}| = |\mathbf{k}_0| \sqrt{\frac{\varepsilon_m \varepsilon_d}{\varepsilon_m + \varepsilon_d}}$ and $|\mathbf{k}_{\text{WA}}| = |\mathbf{k}_0| \sqrt{\varepsilon_d}$, respectively. Here, ε_m and ε_d are the relative dielectric constants of metal and surrounding medium [39]. Then we consider electromagnetic modal properties of the periodic plasmonic-photonic hybrid system shown in Figure 1A. In Figure 2A, we have shown the evolutions of resonant response in the hybrid system together with the increasing lattice constant revealed by the random ED excitation methods (see Methods and Supporting Information, Figures S1 and S2 for details). As we can see in Figure 2A, the dependences of k_{SPP} and k_{WA} on the lattice constant of the array are presented by red dots and white dashed line, which show very good correspondences to two modes found by the random ED excitation method and identifies the SPP and WA modes of the hybrid system, respectively. We also outlined the evolutions of two other modes by black dots and white dots, respectively. For the hybrid structure with a large lattice constant, i.e. $l \sim 1000$ nm, there is a resonance mode whose resonant wavelength (720 nm) is similar to the single particle case shown in Figure 1C. The resonant wavelengths of this mode are hardly changed with the reduction of lattice constant (see black dots), where we name it as the bianisotropic induced mode (BM). The resonant mode indicated by the white dots manifests itself as a Z-oriented ED (p_z) in one

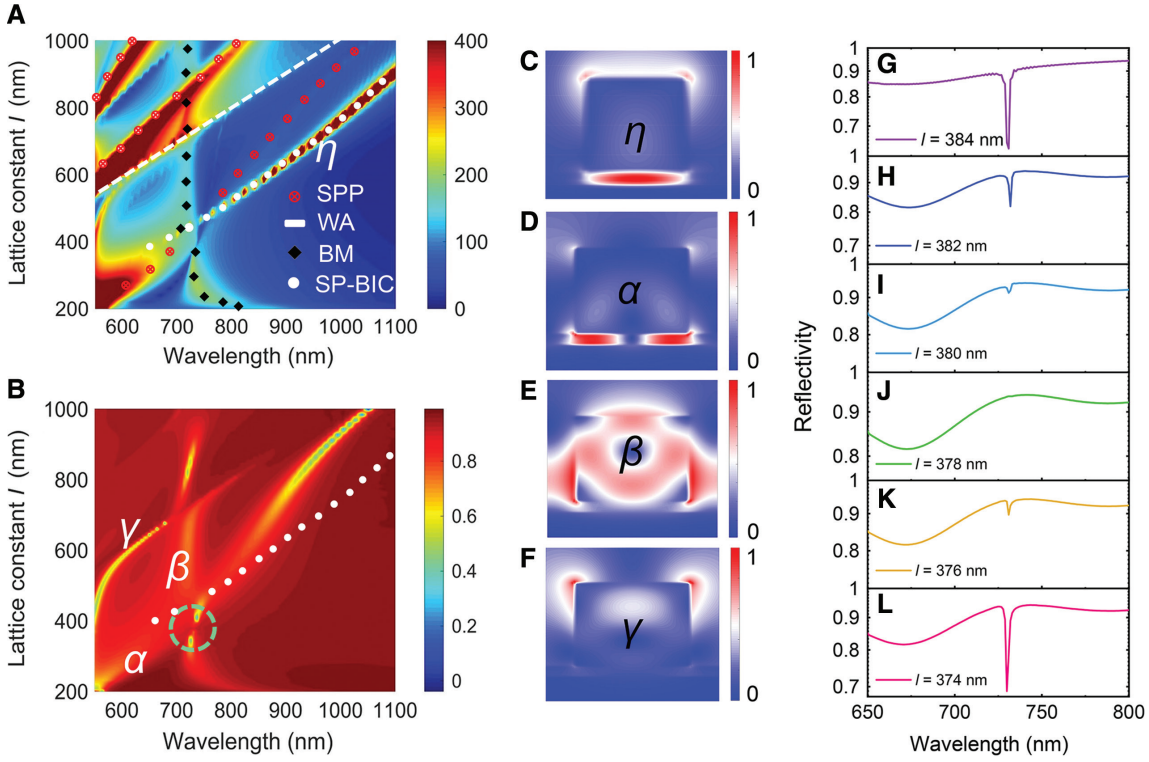

Figure 2: Bound states in the continuum in plasmonic-dielectric hybrid systems.
(A) Resonant modes of the hybrid structure revealed by using randomly oriented and distributed ED sources. (B) Resonant modes revealed in the reflection spectra of a normal incident plane wave (*p*-polarized) calculated for hybrid structures with different lattice constants. The symmetry-protected BIC at the Γ-point, which is not revealed in the reflection spectra, is indicated by the white dots. (C–F) Electric field distributions calculated for the cases marked η, α, β, and γ in (A) and (B), respectively. (F–L) Evolution of the reflection spectra for the FW-BIC with decreasing lattice constant in the range of 374–384 nm.

unit cell, as shown by Figure 2C. In order to further identify other modes excited in the hybrid structure, we have also presented the electric field distributions in a unit cell for different modes marked as α, β and γ in Figure 2B, as shown in Figure 2D–F. The electric field of the α mode localizes in the nanoscale spacer layer between the Si nanopillar and the Ag film, indicating a SPP nature of this mode. The electric field of the mode marked at β is mainly distributed inside the Si nanopillar, manifested itself as the circular electric field distribution inside the nanopillar. It means that such mode is associated with the bianisotropic effect where the ED moment (p_x) of the nanoparticle induces a MD (m_y) moment of the nanoparticle. The resonant wavelengths of the mode marked at β keep almost unchanged together with the increasing of lattice constant (see Figure 2A). In addition, we presented the electric field distribution of the WA mode at γ. As shown in Figure 2E, its electric field is weakly localized at two corners of the Si nanopillar, implying that it is caused by the far-field coupling of the Si nanopillars via the lattice.

In order to evaluate whether these modes can be accessed by a normally incident plane wave, we have further provided the reflection spectra of the hybrid structures with different lattice constants, as shown in Figure 2B. Comparing the results of Figure 2A and B, we clearly found the signatures of two BIC modes in this hybrid system. The first one is the FW-BIC as indicated by a green dashed circle in Figure 2B. It is remarkable that the strong interaction between the SPP mode and the BM creates a region of avoided crossing resonances when the lattice constant is varied from 374 to 384 nm, as shown in Figure 2A and B. The interference between these two resonant modes results in the vanish of linewidth of one resonance. We further provided the reflection spectra in Figure 2G–L, where the dip in the reflection spectrum disappears at l=378 nm, forming the so-called FW-BIC. At the same time, we also noticed that there is a mode (marked by white dots in Figure 2A) that is not revealed in the reflection spectra of the normally incident plane wave shown in Figure 2B. It means that this mode cannot couple to the plane wave propagating along the *Z* direction. As mentioned above, such mode manifests itself as an ED oriented along the *Z* direction in the Si nanopillar, as shown by Figure 2C. This mode can be accessed by an inclined

incident plane wave with suitable polarization that will be discussed in the following, indicating that it is a SP-BIC mode. Different from the BM, the SP-BIC mode shifts to longer wavelengths with increasing lattice constant (see Figure 2A).

In order to gain a deep insight into two kinds of BICs formed in the hybrid structure, we calculated the reflection spectra of the hybrid structure illuminated by a plane wave at different incident angles with the lattice constant $l = 320$ nm. The reflection spectra of the hybrid structure excited by *p*- and *s*-polarized plane wave at different incidence angles are shown in Figure 3A and B, respectively. For the normal incidence case ($\theta = 0°$), the SPP mode appears at ~620 nm. According to Eq (1), its resonant frequency redshifts together with the enlargement of incident angle. As a result, such mode will interact with the BM together increase and an avoided-cross frequency region at ~731 nm appears. The FW-BIC is created when the incident angle reaches $\theta = 22°$. According to Eq. (1), the wave vector of the incident light in the *X*-*Z* plane is enlarged with increase in the incident angle, which is equivalent to the enlargement of the array period. Such process will eventually lead to the formation of FW-BIC similar to the case shown in Figure 2B. In contrast, one can see only the BM at ~731 nm which is almost invariant with the increasing of the incidence angle for *s*-polarized plane wave, because the SPP mode cannot be excited at this case, as shown in Figure 3B. Furthermore, we showed the reflection spectra calculated for a hybrid structure with the lattice constant $l = 700$ nm excited by *p*- and *s*-polarized plane waves in Figure 3C and D, respectively. For the *p*-polarized plane wave, the SP-BIC cannot be accessed at the normal incidence and gradually evolves into leaky resonances when the excitation condition is slightly detuned from the normal incidence. For the *s*-polarized plane wave, however, there is no BIC revealed in the reflection spectra, because SPP associated SP-BIC mode cannot be excited in this case.

In order to show quantitatively, how the Q factors of the BICs can be manipulated, we showed the dependence of the Q factor on the lattice constant of the hybrid structure derived for the FW BIC in Figure 4A. When the lattice constant approaches $l = 378$ nm, the Q factor of the Fano resonance rises dramatically and trends to become divergent. Owning to the absence of radiation loss, the Q factor of the BIC created in the hybrid structure is much larger than that achieved in the WA mode (~100). For the SP-BIC, we can also extract the dependence of Q factor on

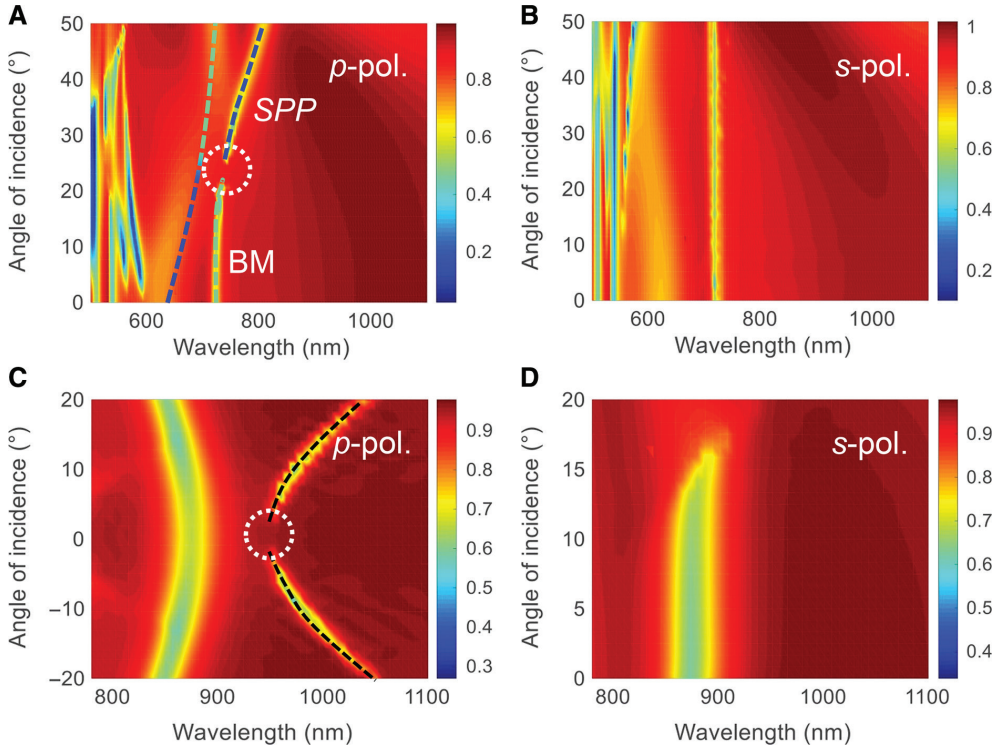

Figure 3: Transitions between BICs and leaky resonances.
Reflection spectra of the hybrid structure with $l = 320$ nm calculated at different incident angles for *p*- and *s*-polarized plane waves are shown in (A) and (B). Reflection spectra of the hybrid structure with $l = 700$ nm calculated at different incident angles for (C) *p*- and (D) *s*-polarized plane waves.

the excitation condition from the angle-resolved reflection spectra, as shown in Figure 4B. It can be seen that the Q factors increase sharply as the incidence angle is reduced to $\theta = 10°$ and a Q factor of ~350 is achieved at $\theta \sim 2°$.

For photonic circuits in the future, Si-based lasers compatible with the current fabrication technology of Si chips are highly desirable. Very recently, efficient white light emission from Si nanoparticles has been achieved by exploiting the excitation and emission enhancements of Mie resonances with femtosecond laser pulses [7]. The strongly localized electric field inside the nanoparticle achieved at the MD resonances of a Si nanoparticle significantly enhances the two- and three-photon-induced absorption (2PA and 3PA) of the Si nanoparticle, leading to the emission of hot electron luminescence. As the Q factors of Mie resonances are quite low, it is anticipated that one can enhance the Q factor of the system, while maintaining similar electric field distribution as the MD mode of a Si nanoparticle. Since the 2PA and 3PA of a Si nanoparticle are found to be related to the integration of $|E|^4$ and $|E|^6$ over the volume of the Si nanoparticle, the FW-BIC associated resonance provides an unique opportunity to boost the Q factor of the structure while maintaining the effective mode volume of the constituent Si nanoparticle comparable to a single Si nanoparticle case simultaneously. It should be pointed out that the effective mode volume mentioned here in one unit cell of the structure is analogue to the definition of a single Si nanopillar. We therefore examine the enhancement factor of nonlinear optical absorption in the Si nanopillar of the hybrid structure($l = 365$ nm) which is close to the FW-BIC condition ($l = 378$ nm). In this case, the hybrid structure is excited by using a plane wave propagating along the -Z direction. As shown in Figure 5A, very large 2PA and 3PA enhancement can be achieved at ~730 nm where the leaky resonance associated with the FW-BIC appears. The corresponding electromagnetic field distribution for this leaky resonance is shown in the inset of Figure 5B, where the electromagnetic field is mainly located inside the nanoparticle, leading to enhancement factors as large as 3500 and 250 for the 3PA and 2PA compared with the single dielectric nanoparticle case, respectively. We also examine the dependence of the 2PA and 3PA on the lattice constant of the hybrid structure, as shown in Figure 5B. Significant enhancement of the 2PA and 3PA of Si nanopillars can also be achieved in the hybrid structures close to the FW-BIC condition owing to the dramatical increase of radiative Q factor.

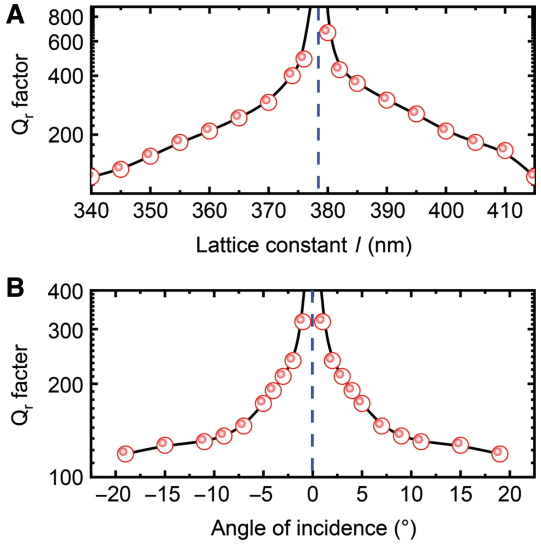

Figure 4: Divergence of Q factor at the BIC conditions. (A) Dependence of Q factors on the lattice constant of the hybrid structure for the normal incident plane wave. (B) Dependence of the Q factors on the incident angle calculated for the hybrid structure with $l = 700$ nm. The open circles represent the calculated Q factor while solid lines are guide for the eye.

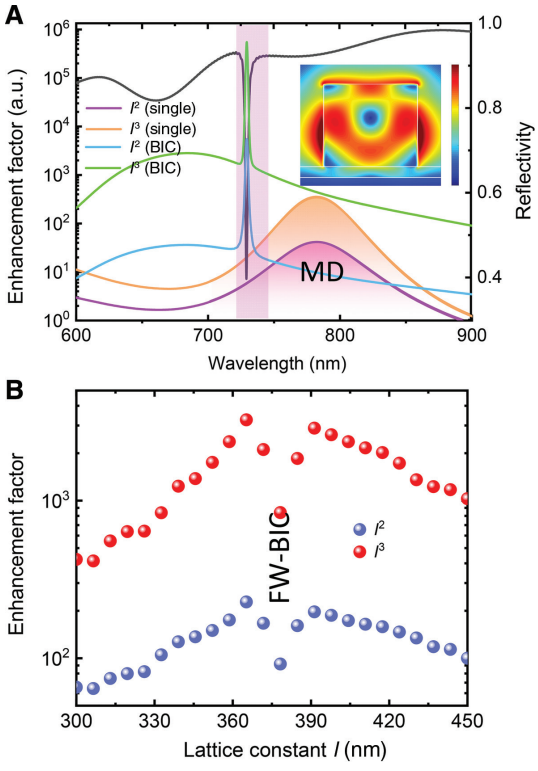

Figure 5: Electric field enhancement mediated by FW-BIC. (A) Reflection spectrum of the hybrid structure with the lattice constant $l = 365$ nm which is close to the FW-BIC condition ($l = 378$ nm). Here, we present the 2PA and 3PA by $I^2 = \frac{1}{V}\int |E|^4 dV$ and $I^3 = \frac{1}{V}\int |E|^6 dV$. The electric field distribution in a unit cell of the periodic structure is shown in the inset. (B) Dependence of the nonlinear optical absorption (2PA and 3PA) on the lattice constant. It is normalized to the single dielectric particles case.

In addition to confine electromagnetic field inside the dielectric nanoparticles, the electric field can also be strongly localized in the nanoscale MgF_2 layer, if we selectively excite the SP-BIC of the hybrid structure, as shown in Figure 2C. In order to show the advantage of the proposed hybrid structure over the all-dielectric structure composed of the regular array of Si nanopillars only (i.e. without the spacer layer and Ag film), we have presented the reflection spectra for the same all-dielectric structures first, as shown in Figure 6A. In this case, the all-dielectric structures are excited by using a plane wave propagating along the -*Z* direction. As discussed above, the SP-BIC cannot be excited by using a normal incident plane wave. While it can be revealed by using randomly oriented and distributed ED sources inside the structure, as shown in Figure 6B. For comparison, the reflection spectra and the resonant modes revealed by using randomly oriented and distributed ED sources are presented in Figure 6C and D. In the absence of the Ag film, only the SP-BICs can be found in all-dielectric structure. In Figure 6E, we have presented the electric field distribution in one unit cell of the structure calculated at the SP-BIC of an all-dielectric structure with the lattice constant $l = 700$ nm (see Figure 6B). It is found that the dominated ED moment inside the Si nanopillar is along the *Z* direction, belonging to a p_z SP-BIC mode. In sharp contrast, the electric field is strongly localized in the spacer layer between the Si nanopillar and the Ag film for the SP-BIC supported in the hybrid structure with a nanoscale MgF_2 layer of $g = 5$ nm (see Figure 6E, F and G). At the same time, the effective mode volume in one unit cell of the infinite structure can be reduced by one order of magnitude as compared with the all-dielectric structure, which exhibits strong dependence on the gap width between the Si nanopillar and the Ag film, as shown in Figure 6H (see Supporting Information, Figure S3). For $g = 1$ nm, 10 times reduction of the effective mode volume can be achieved, which is very useful for the study of light-matter interaction in two-dimensional material. A detailed investigation reveals that the electric field in the *Z* direction (E_z) is three orders of magnitude larger than that in the *X* direction (see Supporting Information, Figure S4). It implies that the Purcell factor for out-of-plane dipoles can be several orders of magnitude larger than that for in-plane dipoles. The large asymmetry in the electric field offers the opportunity for detecting the dark excitons in two-dimensional materials by using the SP-BIC in the hybrid structure, which remains a big challenge at present [40]. The proposed structure can be fabricated utilizing a generalization of the fabrication process presented in [41]. It should be pointed out that a special attention should be paid to the whole fabrication process to guarantee the quality of MgF_2 layer similar to Ref. [10], as fabricating a

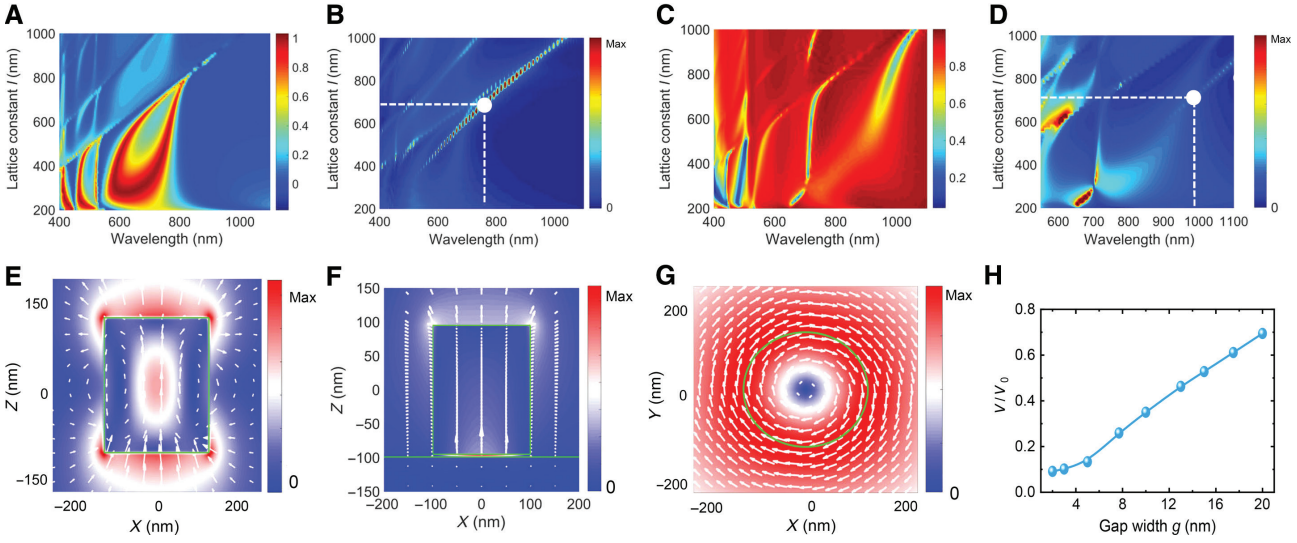

Figure 6: Localization effect of electromagnetic field mediated by SP-BIC.
Reflection spectra calculated for all-dielectric structures (A) and hybrid structures (C) with different lattice constants by using a normal incident plane wave. The electromagnetic modal responses revealed in all-dielectric and hybrid structures by using randomly oriented and distributed ED sources are shown in (B) and (D), respectively. In each case, the dashed lines indicate the lattice constant of the Si nanopillars and the resonant wavelength of the BIC. (E) The electric field distribution and the corresponding in-plane electric field vectors at the *XZ* plane calculated for the SP-BIC of the all-dielectric structure with the lattice constant $l = 700$ nm. (F) and (G) The electric field distributions at the *XZ* and *XY* planes and the corresponding in-plane electric field vectors calculated for the SP-BIC of the hybrid structure with the lattice constant $l = 700$ nm. (H) Dependence of the effective mode volume of the unit cell on the width of the nanoscale MgF_2 layer calculated for the lattice constant $l = 700$ nm. It is normalized to the effective mode volume of the unit cell V_0 in the all-dielectric case.

uniform nanometer scale film is still challenging. Such sub-nanoscale layer can be substituted by 2D materials, which have been demonstrated recently [42]. Note that this proposed effect is valid when taking the absorption of Si in the visible spectrum into account [43]. (see Supporting Information, Figure S5). It should be pointed out that the topological protected BIC can be used against the fabrication disorder and substantially maintain high radiative Q factors in realistic devices [44–46].

3 Concluding remarks

In summary, we have proposed a novel hybrid dielectric-metal structure supporting symmetry protected and Friedrich-Wintgen BIC to effectively compress the mode volume of BIC mode regarding to the all-dielectric system. It is found that the Friedrich-Wintgen BIC originates from the strong coupling between the bianisotropic effect induced mode and the SPP of the hybrid structure, whose electric field is mainly localized inside the dielectric naonparticle. Three and two orders of magnitude enhancement in three photon and two photon absorption can be realized utilizing the Friedrich-Wintgen BIC compared with the single nanoparticle case. While the symmetry protected BIC is originated from the *Z*-oriented EDs in the unit cells of the array, whose electric field is strongly localized in the nanoscale spacer region. Such a symmetry protected BIC mode of the hybrid system processes a mode volume in one order of magnitude smaller than the conventional SP-BIC of the all-dielectric case. By selectively exciting the symmetry protected BIC or Friedrich-Wintgen BICs supported in the hybrid system, the BIC associated spatial localization and enhancement of electric field in the hybrid structure can be manipulated effectively. The hybrid structure proposed in this work offers the unique possibility for controlling and enhancing light-matter interaction in the high-Q resonance region, which offers feasibility for tailoring nonlinear optical absorption, harmonic generation, lasing, dark exciton, and beyond.

4 Methods

4.1 Numerical modeling

The scattering spectra of Si nanoparticles placed on a substrate were calculated by using the finite-difference time domain (FDTD) method. In the FDTD simulation, a nonuniform mesh with the smallest mesh size of 2 nm as well as a perfectly matched boundary condition was employed. Then we can decompose the contributions of induced electromagnetic multipolar moments in the Si nanoparticle to the extinction cross sections [34]. In this case, the electric dipole (ED) and magnetic dipole (MD) moments induced in the Si NS can be calculated based on the electric field $\mathbf{E}(\mathbf{r})$, i.e. $\mathbf{p}=\int\mathbf{P}d\mathbf{r}$, $\mathbf{m}=\int\mathbf{r}\times\mathbf{P}d\mathbf{r}$, $\mathbf{P}=\varepsilon_0(\varepsilon_p-\varepsilon_d)\mathbf{E}$. Here, ε_0 is the permittivity of vacuum, ε_p and ε_d are the relative permittivity of nanoparticle (Si in our case) and environment (air in our case), respectively. In our case, the extinction cross section contributed by the induced ED and MD moments under the excitation of a *X*-polarized plane wave can be written as: [34]

$$\sigma_{\text{ext}}=\frac{k_d}{\varepsilon_0\varepsilon_d}\text{Im}\left(E_{0x}^{\star}\left(p_x+\frac{1}{c}m_y\right)\right)$$

Here, k_d is the wave vector of the incident plane wave in the surrounding medium. c is the velocity of light.

In order to reveal the resonance modes of the hybrid structure which cannot be accessed by the normalincident plane wave, we use 10 randomly oriented and distributed ED sources dispersed in one unit cell of the hybrid structure to effectively excite all the resonant modes. Then we record the time evolution of electric field at 7 randomly distributed locations in the unit cell, where the numbers of locations are sufficient to extract the modal properties even some of them are accidentally located at the node of an electromagnetic mode. The response of the system in frequency domain can be obtained through the average of Fourier transformation results of the recorded time-domain signals (see Supporting Information, Figures S1 and S2). In the calculation, periodic boundary conditions are applied at the planes perpendicular to the *X* and *Y* axes while perfect matching layers are used in the *Z* direction. It should be pointed out that we apodize the time signals by applying a Gaussian-shaped window to filter out the excitation signal. The permittivity of Ag was modelled using the experimental data reported in [47] and the refractive index of silicon was taken in [43]. The effective mode volume of the plasmonic cavity modes can be expressed as [12, 48]:

$$V_{\text{mode}}=\frac{\int\varepsilon(r)E^2dV}{\max(\varepsilon(r)E^2)}$$

where $\varepsilon(r)$ is the material dielectric constant. The electric field intensity was integrated over the entire mode structure.

Acknowledgment: The authors acknowledge the financial support from the National Key Research and Development Program of China (No. 2016YFA0201002), the National Nature and Science Foundation of China (Nos. 11674110,

11874020, 11674130 and 91750110), the Natural Science Foundation of Guangdong Province, China (Grant Nos. 2016A030308010, 2016A030306016 and 2016TQ03X981), the Science and Technology Planning Project of Guangdong Province, China (Grant No. 2015B090927006) and the Pearl River Nova Program of Guangzhou (No. 201806010040).

References

[1] Chikkaraddy R, de Nijs B, Benz F, et al. Single-molecule strong coupling at room temperature in plasmonic nanocavities. Nature 2016;535:127–30.
[2] Liu R, Zhou ZK, Yu YC, et al. Strong light-matter interactions in single open plasmonic nanocavities at the quantum optics limit. Phys Rev Lett 2017;118:237401.
[3] Baranov DG, Wersall M, Cuadra J, Antosiewicz TJ, Shegai T. Novel nanostructures and materials for strong light matter interactions. ACS Photonics 2018;5:24–42.
[4] Kelly KL, Coronado E, Zhao LL, Schatz GC. The optical properties of metal nanoparticles: The influence of size, shape, and dielectric environment. J Phys Chem B 2003;107:668–77.
[5] Kravets VG, Kabashin AV, Barnes WL, Grigorenko AN. Plasmonic surface lattice resonances: a review of properties and applications. Chem Rev 2018;118:5912–51.
[6] Ha ST, Fu YH, Emani NK, et al. Directional lasing in resonant semiconductor nanoantenna arrays. Nat Nanotechnol 2018;13:1042.
[7] Zhang C, Xu Y, Liu J, et al. Lighting up silicon nanoparticles with Mie resonances. Nat Commun 2018;9:2964–4.
[8] Xiang J, Jiang S, Chen J, et al. Hot-electron intraband luminescence from GaAs nanospheres mediated by magnetic dipole resonances. Nano Lett 2017;17:4853–9.
[9] Xiang J, Li J, Zhou Z, et al. Manipulating the orientations of the electric and magnetic dipoles induced in silicon nanoparticles for multicolor display. Laser Photonics Rev 2018;12:1800032.
[10] Oulton RF, Sorger VJ, Zentgraf T, et al. Plasmon lasers at deep subwavelength scale. Nature 2009;461:629–32.
[11] Oulton RF, Sorger VJ, Genov DA, Pile DFP, Zhang X. A hybrid plasmonic waveguide for subwavelength confinement and long-range propagation. Nat Photonics 2008;2:496–500.
[12] Chang-Hee C, Aspetti CO, Park J, Agarwal R. Silicon coupled with plasmon nanocavities generates bright visible hot luminescence. Nat Photonics 2013;7:285–9.
[13] Xifre-Perez E, Shi L, Tuzer U, et al. Mirror-image-induced magnetic modes. ACS Nano 2013;7:664–8.
[14] Li H, Xu Y, Xiang J, et al. Exploiting the interaction between a semiconductor nanosphere and a thin metal film for nanoscale plasmonic devices. Nanoscale 2016;8:18963–71.
[15] Chen S, Zhang Y, Shih TM, et al. Plasmon-induced magnetic resonance enhanced raman spectroscopy. Nano Lett 2018;18:2209–16.
[16] von Neumann J, Wigner E. Uber merkwürdige diskrete Eigenwerte. Phys Z 1929;30:465–7.
[17] Marinica DC, Borisov AG, Shabanov SV. Bound states in the continuum in photonics. Phys Rev Lett 2008;100:183902.
[18] Bulgakov EN, Sadreev AF. Bound states in the continuum in photonic waveguides inspired by defects. Phys Rev B 2008;78:075105.
[19] Hsu CW, Zhen B, Lee J, et al. Observation of trapped light within the radiation continuum. Nature 2013;499:188–91.
[20] Yang Y, Peng C, Liang Y, Li Z, Noda S. Analytical perspective for bound states in the continuum in photonic crystal slabs. Phys Rev Lett 2014;113:037401.
[21] Bulgakov EN, Sadreev AF. Bloch bound states in the radiation continuum in a periodic array of dielectric rods. Phys Rev A 2014;90:053801.
[22] Hsu CW, Zhen B, Ston AD, Joannopoulos JD, Soljačić M. Bound states in the continuum. Nat Rev Mater 2016;1:16048.
[23] Carletti L, Koshelev K, De Angelis C, Kivshar Y. Giant nonlinear response at the nanoscale driven by bound states in the continuum. Phys Rev Lett 2018;121:033903.
[24] Dai S, Liu L, Han D, Zi J. From topologically protected coherent perfect reflection to bound states in the continuum. Phys Rev B 2018;98:081405.
[25] He Y, Guo G, Feng T, Xu Y, Miroshnichenko AE. Toroidal dipole bound states in the continuum. Phys Rev B 2018;98:161112.
[26] Yanik AA, Cetin AE, Huang M, et al. Seeing protein monolayers with naked eye through plasmonic Fano resonances. Proc Natl Acad Sci USA 2011;108:11784–9.
[27] Kodigala A, Lepetit T, Gu Q, Bahari B, Fainman Y, Kante B. Lasing action from photonic bound states in continuum. Nature 2017;541:196–9.
[28] Tikhodeev SG, Yablonskii AL, Muljarov EA, et al. Quasiguided modes and optical properties of photonic crystal slabs. Phys Rev B 2002;66:045102.
[29] Christ A, Tikhodeev SG, Gippius NA, et al. Waveguide-plasmon polaritons: strong coupling of photonic and electronic resonances in a metallic photonic crystal slab. Phys Rev Lett 2003;91:183901.
[30] Friedrich H, Wintgen D. Interfering resonances and bound states in the continuum. Phys Rev A 1985;32:3231.
[31] Rybin MV, Koshelev KL, Sadrieva ZF, et al. High-Q supercavity modes in subwavelength dielectric resonators. Phys Rev Lett 2017;119:243901.
[32] Bogdanov AA, Koshelev KL, Kapitanova PV, et al. Bound states in the continuum and Fano resonances in the strong mode coupling regime. Adv Photonics 2019;1:016001.
[33] Azzam SI, Shalaev VM, Boltasseva A, Kildishev AV. Formation of bound states in the continuum in hybrid plasmonic-photonic systems. Phys Rev Lett 2018;121:253901.
[34] Evlyukhin AB, Fischer T, Reinhardt C, Chichkov BN. Optical theorem and multipole scattering of light by arbitrarily shaped nanoparticles. Phys Rev B 2016;94:205434.
[35] Evlyukhin AB, Bozhevolnyi SI. Resonant unidirectional and elastic scattering of surface plasmon polaritons by high refractive index dielectric nanoparticles. Phys Rev B 2015;92:245419.
[36] Miroshnichenko AE, Evlyukhin AB, Kivshar YS, Chichkov BN. Substrate-induced resonant magnetoelectric effects for dielectric nanoparticles. ACS Photonics 2015;2:1423–8.
[37] Sinev I, Iorsh I, Bogdanov A, et al. Polarization control over electric and magnetic dipole resonances of dielectric nanoparticles on metallic films. Laser Photonics Rev 2016;10:799–806.
[38] Zou C, Withayachumnankul W, Shadrivov IV, Kivshar YS, Fumeaux C. Directional excitation of surface plasmons by dielectric resonators. Phys Rev B 2015;91:085433.
[39] Shen Y, Zhou J, Liu T, et al. Plasmonic gold mushroom arrays with refractive index sensing figures of merit approaching the theoretical limit. Nat Commun 2013;4:2381.

[40] Park KD, Jiang T, Clark G, Xu X, Raschke MB. Radiative control of dark excitons at room temperature by nano-optical antenna-tip Purcell effect. Nat Nanotechnol 2018;13:59–64.
[41] Liu J, Su R, Wei Y, et al. A solid-state source of strongly entangled photon pairs with high brightness and indistinguishability. Nat Nanotechnol 2019;14:586.
[42] Li Z, Liu C, Rong X, et al. Tailoring MoS_2 Valley-polarized photoluminescence with super chiral near-field. Adv Mater 2018;30:1801908.
[43] Palik ED. Handbook of optical constants of solids. New York, Academic Press, 1998.
[44] Zhen B, Hsu CW, Lu L, Stone AD, Soljačić M. Topological nature of optical bound states in the continuum. Phys Rev Lett 2014;113:257401.
[45] Bulgakov EN, Maksimov DN. Topological bound states in the continuum in arrays of dielectric spheres. Phys Rev Lett 2017;118:267401.
[46] Jin J, Yin X, Ni L, Soljačić M, Zhen B, Peng C. Topologically enabled ultrahigh-Q guided resonances robust to out-of-plane scattering. Nature 2019;547:501–4.
[47] Johnson PB, Christ RW. Optical constants of the noble metals. Phys Rev B 1972;6:4370.
[48] Kristensen PT, Hughes S. Modes and mode volumes of leaky optical cavities and plasmonic nanoresonators. ACS Photonics 2014;1:2–10.

Supplementary Material: The online version of this article offers supplementary material (https://doi.org/10.1515/nanoph-2019-0341).